Journal of Materials Chemistry A

A universal method to form the equivalent ohmic contact for efficient solution-processed organic tandem solar cells

Journal:	*Journal of Materials Chemistry A*
Manuscript ID:	TA-ART-06-2014-003182
Article Type:	Paper
Date Submitted by the Author:	23-Jun-2014

Complete List of Authors:	Li, Ning; Friedrich-Alexander University Erlangen and Nuremberg, Institute Materials for Electronics and Energy Technology, Stubhan, Tobias; FAU Erlangen, WW6 Krantz, Johannes; FAU Erlangen, WW6 Machui, Florian; University Erlangen, Institute Materials for Electronics and Energy Technology Turbiez, Mathieu; BASF, Ameri, Tayebeh; University Erlangen, Institute Materials for Electronics and Energy Technology, Brabec, Christoph; Friedrich-Alexander-Universität Erlangen-Nürnberg, Institute Materials for electronics and energy technology

Journal Name

RSCPublishing

ARTICLE

A universal method to form the equivalent ohmic contact for efficient solution-processed organic tandem solar cells

Cite this: DOI: 10.1039/xoxxoooooox

Received ooth January 2012,
Accepted ooth January 2012

DOI: 10.1039/xoxxoooooox

www.rsc.org/

Ning Li,[*a] Tobias Stubhan,[a] Johannes Krantz,[a] Florian Machui,[a] Mathieu Turbiez,[b] Tayebeh Ameri[a] and Christoph J. Brabec[a,c] ,

The highly transparent, conductive and robust intermediate layer (IML) is the primary challenge for constructing efficient organic tandem solar cells. In this work, we demonstrate an easy but generic approach to realize the fully functional, solution-processed IMLs. In detail, solution-processed silver-nanowires are packed at low concentration between hole- and electron-transporting layer to convert an otherwise rectifying interface into an ohmic interface. The IMLs are proven to be of ohmic nature under applied bias, despite the unipolar charge selectivity of the single layers. Ohmic recombination within IMLs is further proven in organic tandem solar cells fabricated by doctor-blading under ambient conditions. The tandem solar cells based on PCDTBT:[70]PCBM as bottom cell and pDPP5T-2:[60]PCBM as top cell give a power conversion efficiency of 7.25%, which is among the highest values for solution-processed organic tandem solar cells fabricated by using a roll-to-roll compatible deposition method in air.

Introduction

The rapid growth in the field of organic photovoltaics (OPV) has attracted more and more attention from worldwide researchers during the last decade due to its large-scale, low-cost and easy manufacturing properties.[1-6] It has been reported that the power conversion efficiency (PCE) of OPV devices has already surpassed the 10% milestone, which shows enormous promise and potential for commercial applications.[7,8] The PCE limitations of OPV devices are mainly due to the narrow absorption spectra of the donor materials, resulting in decreased short circuit current density (Jsc) and the thermalization losses, resulting in decreased open circuit voltage (Voc).[9,10] The reduced Jsc can be addressed by ternary or multicomponent donor-acceptor systems, which were successfully shown to broaden the absorption of organic semiconductor composites.[11-13] The thermalization losses are more complex to tackle. Hummelen et al. recently suggested the design of organic semiconductors with high dielectric constant to reduce losses related to the exciton binding energy.[14] Another approach is the tandem concept, which stacks two or more cells with complementary absorption spectra in series or parallel connection. This concept addresses both losses: the Jsc related absorption losses as well as the Voc related thermalization losses. In the last few years, a number of organic tandem solar cells with high efficiencies were reported,[8, 15-22] and the efficiency roadmap for tandem cells is clearly pointing towards the predicted 15%.[23]

To realize high performance organic tandem solar cells, an efficient and reliable intermediate layer (IML) is required, which is typically designed from a series-connected sequence of a hole-transporting layer (HTL) and an electron-transporting layer (ETL).[22] The performance of an organic tandem solar cell is strongly dependent on the quality and functionality of its IML. Ideally, the IML should be highly transparent, conductive and robust enough to protect the underlying semiconductor layer and to form a quasi ohmic contact between HTL and ETL.[24] The majority of novel active layer materials are sensitive to humidity and oxygen at elevated temperatures and the microstructure of the semiconductor layer might be negatively influenced by the high temperature processing. Therefore the fabrication of efficient organic tandem solar cells including the IML should avoid high temperature steps.[25]

Although many efforts have been made to understand the recombination properties of IMLs, utilizing commonly used buffer layers to form the quasi ohmic contact in a general way is still a problem for solution-processed tandem solar cells. Today´s reference materials for the IMLs are Poly(3,4-ethylenedioxythiophene):poly(styrenesulfonate) (PEDOT:PSS) for the hole injection and either titanium oxide (TiOx) [26] or zinc oxide (ZnO) [8,15-20] for the electron injection. Solution-

processed p-type metal oxides, such as vanadium pentoxide (V_2O_5),[27,28] molybdenum trioxide (MoO_3) [29,30] and tungsten trioxide (WO_3),[31,32] were reported as substitutions for the widely used PEDOT:PSS, owing to the comparable device performances but enhanced environmental lifetime for single-junction solar cells.[33,34] However, the commonly used n- and p-type interface layers, such as PEDOT:PSS and intrinsic metal oxides, do not necessarily form a quasi ohmic contact, especially for the direct contact between metal oxides and metal oxides. Although several groups reported the necessity to thermally-evaporate an ultra-thin metal layer (Au, Ca, or Al) between the HTL and ETL,[35-37] the combination of solution processing with vacuum processing is unattractive for up-scaling and low-cost fabrication. Moreover, the mandatory oxygen plasma or ozone pretreatment activation, specifically relevant for many current p-type metal oxides like for MoO3 or NiO, is incompatible to tandem processing.[29,38] Nowadays, solution-processed IMLs reported by several research groups were mainly based on highly conductive PEDOT:PSS, which were exclusively modified to certain n-type interface layers, such as ZnO, to form the quasi ohmic contact.[8,15-20] Solution-processed ZnO nanoparticles (ZnO-np) are not well defined in terms of their electrical and semiconducting properties (density of states and density of charge carriers) and may differ for various processes and routes.[24,39] Moreover, the chemical nature and the density of the ligand groups terminating the surface of ZnO-np, which is essential for contact/interface formation, is very difficult to assess and not known for most systems.

Low-temperature solution-processed metallic nanowires were recently reported as a promising transparent electrode and a potential substitute for sputtered ITO and thermally-evaporated top electrode.[40-43] Metallic nanowire electrodes impress with high conductivity and high transparency, coupled with easy manufacturing. In this manuscript we demonstrate an easy but generic approach to fully solution-processed efficient IMLs at fairly low temperatures ($\leqslant 80^\circ$ C). In detail, a solution-processed thin silver-nanostructure layer, coated from highly diluted silver-nanowire (AgNW) solution between the p-type and n-type charge transporting layer, is able to form an ohmic recombination contact between otherwise non-ohmic semiconductors. The generic approach of this concept is verified at the hand of two very different HTL/ETL recombination layers, on the one hand a PEDOT:PSS/ZnO-np layer and on the other hand a WO_3/ZnO-np layer. It is again worthwhile to highlight that the fully functional solution-processed IMLs have been reported by several research groups for efficient tandem solar cells, however, the specific interface materials requirements as well as the strict processing conditions restricted the reproduction of the reported promising results. Therefore, the universal approach demonstrated in this contribution indicates the way of forming equivalent ohmic contact between arbitrary qualified n- and p-type interface layers for efficient IMLs, which significantly reduces the workload of screening qualified interface materials for solution-processed organic tandem solar cells.

Results and discussion

The charge recombination property of IMLs is investigated in the single-junction OPV devices, as illustrated in Figure 1(a), which gives immediate feedback on the ohmic nature of the IMLs.[24,39] To match the requirements of IML for efficient tandem solar cells, the holes and electrons that are selectively extracted by HTL and ETL should efficiently recombine at the interface. In this case, the single-junction devices with the recombination layers are supposed to show the same performance as devices with a single interface layer.[24] Figures 1(b) and (c) represent the transmission spectra of the thin layers and chemical structures of active materials used in this work. PEDOT:PSS AI4083 was purchased from Heraeus and diluted in isopropyl alcohol (IPA) at a volume-ratio of 1:5 before processing. ZnO-np were synthesized from zinc acetate [44] and dissolved in ethanol at 2 wt.-%. WO_3 nanoparticles were synthesized from flame pyrolysis [31,32] and dissolved at 2.5 wt.-% in ethanol. The AgNW ink was prepared from a water based master solution and diluted in IPA at a volume-ratio of 1:5 (AgNW 1) or 1:10 (AgNW 2). The AgNW 1 and AgNW 2 are highly transparent, as depicted in Figure 1(b) inset. In the configuration measured, and after correction of the substrate, transmission values of over 99% are observed in a wavelength range from 350 to 600 nm. A full analysis of the optical properties of AgNW films is reported elsewhere.[40] The metal oxides WO_3 and ZnO-np absorb in the blue regime, while PEDOT:PSS is more absorbing in the infrared regime. Overall transmission of the charge extraction layers is >90%.

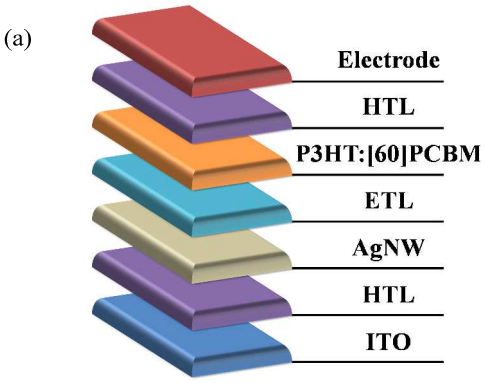

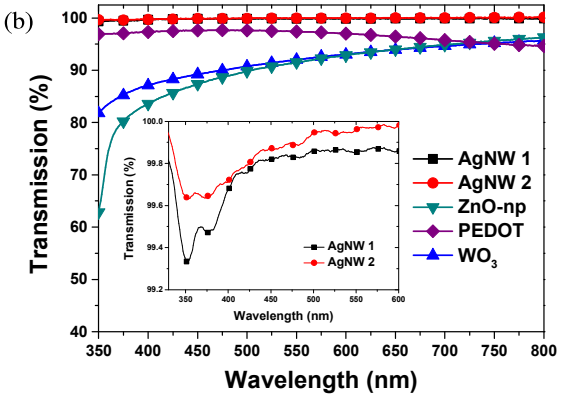

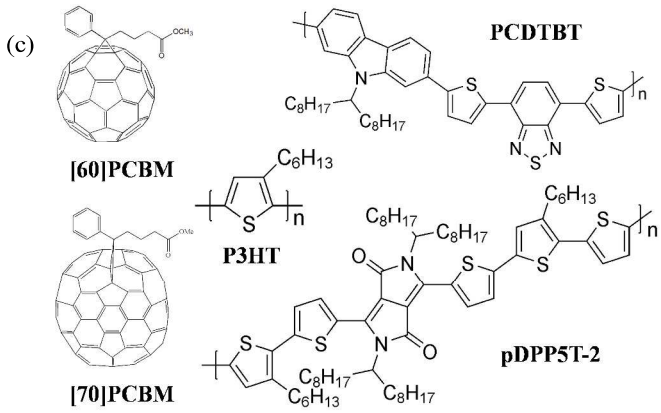

Figure 1 (a) Architecture of the single-junction solar cells with a solution-processed intermediate layer; (b) Transmission spectra of hole- and electron-transporting layers. AgNW was diluted in IPA at a volume-ratio of 1:5 for AgNW 1 or 1:10 for AgNW 2; (c) Chemical structures of active materials used in this work.

Poly(3-hexylthiophene):[6,6]-phenyl-C61 butyric acid methyl ester (P3HT:PCBM) with a thickness of 100 nm was used as active layer. The J-V characteristics of the corresponding OPV devices are summarized in Figure 2 and Table 1. As depicted in Figure 2(a), we find significant limitations for the PEDOT:PSS/ZnO-np interface. Most obvious is the rather low injection under forward bias, resulting in a low fill factor (FF). Consequently, this recombination layer is not expected to properly work in a tandem configuration. Nevertheless, all these problems can be overcome by employing the solution-processed Ag nanostructure-based thin layer, which completely lifts the recombination restrictions at HTL/ETL interface. The organic solar cells incorporating AgNW-based recombination layer (Device C and D) exhibit comparable performance with the reference (Device A). As shown in Figure 2(c), the single-junction solar cells comprising an IML of WO_3/ZnO-np (Device E) suffer from the same deficiencies as the PEDOT:PSS/ZnO-np devices (Device B), namely low rectification from a high series resistance. Similarly, the performance of the devices utilizing the WO_3/ZnO-np IML was again significantly improved by inserting AgNW at the interface. In the case of WO_3, a more distinct difference was observed for AgNW 1 versus AgNW 2. Device F, employing the WO_3/AgNW 1/ZnO-np IML suffers from a significantly higher shunt than Device G with the WO_3/AgNW 2/ZnO-np interface. Furthermore, in comparison with the reference devices, the performances of the single-junction solar cells with HTL/AgNW/ETL injection layer were not affected by the optical losses in the IMLs. In contrast, the single-junction solar cells employing the AgNW-based IML exhibit even slightly higher Jsc compared with the reference device employing a pristine ZnO-np layer, which may be caused by either small variation in the active layer thickness or by a change in the morphological properties of ZnO-np layer.[46, 47] Summarizing the single-junction devices, it is most relevant to notice that the series resistances (R_S) of OPV devices, as shown in Table 1, were significantly reduced by inserting AgNW 2 at the interface of the IMLs, while the leakage current was still in the same range as that of reference devices, indicating that the recombination property of IML was significantly improved by inserting this ultrathin AgNW layer. The nanoparticles, degraded from nanowires, serve even more efficiently as recombination centers at the interface of HTL/ETL compared with nanowires due to their better shunt. Moreover, if several nanowires overlap each other, as shown in Figure 2(b), this AgNW layer may not be fully covered by overlying 100 nm ZnO-np resulting in high leakage current in the OPV device, which can be observed in the J-V characteristic of Device F.

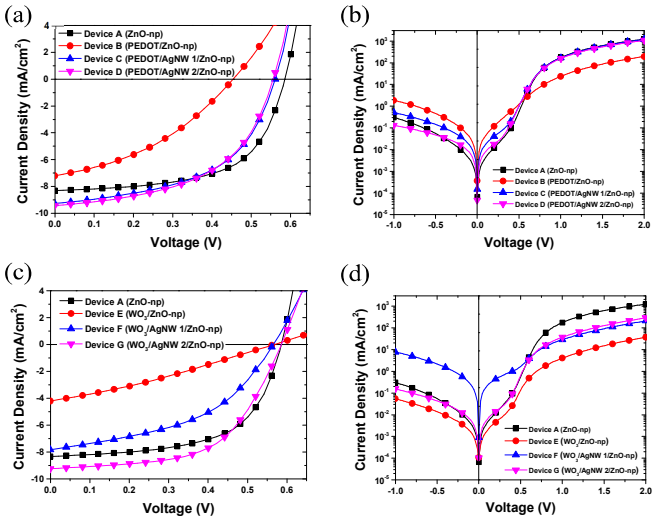

Figure 2 J-V characteristics of single-junction solar cells employing different intermediate layers: (a) and (c) under AM1.5 illumination; (b) and (d) in dark. Device A: ZnO-np layer; Device B: PEDOT:PSS/ZnO-np; Device C: PEDOT:PSS/AgNW 1/ZnO-np; Device D: PEDOT:PSS/AgNW 2/ZnO-np; Device E: WO_3/ZnO-np; Device F: WO_3/AgNW 1/ZnO-np; Device G: WO_3/AgNW 2/ZnO-np.

Table 1 Photovoltaic parameters of single-junction solar cells employing different interlayers. Rs and Rp were calculated from the corresponding J-V characteristics in dark at 0 and 2 V, respectively. The photovoltaic parameters distributions of Device B-G are summarized in Figure S1.

	Interlayer	V_{OC} [V]	J_{SC} [mA/cm^2]	FF [%]	PCE [%]	R_S [Ω cm^2]	R_P [kΩ cm^2]
Device A	ZnO-np	0.58	-8.32	61	2.92	0.82	23.95
Device B	PEDOT:PSS/ZnO-np	0.46	-7.21	37	1.24	4.61	2.32
Device C	PEDOT:PSS/AgNW 1/ZnO-np	0.56	-9.28	52	2.72	0.84	5.66
Device D	PEDOT:PSS/AgNW 2/ZnO-np	0.56	-9.42	51	2.72	0.93	12.52
Device E	WO_3/ZnO-np	0.56	-4.20	30	0.70	22.1	57.31
Device F	WO_3/AgNw 1/ZnO-np	0.56	-7.82	46	2.03	4.25	0.43
Device G	WO_3/AgNW 2/ZnO-np	0.58	-9.24	58	3.10	3.01	16.71

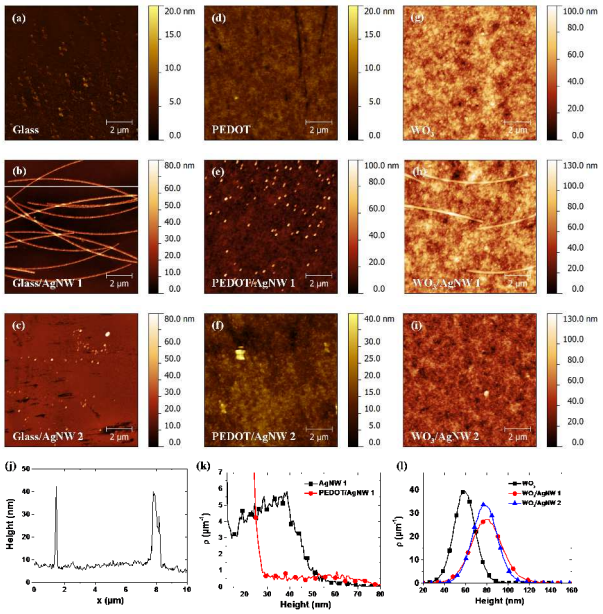

Figure 3 AFM images of different interface layers (scale bar 2 µm): (a) bare glass; (b) AgNW 1 (1:5 vol.% in IPA) on glass; (c) AgNW 2 (1:10 vol.-% in IPA) on glass; (d) 50 nm thick PEDOT:PSS on glass; (e) AgNW 1 on PEDOT:PSS; (f) AgNW 2 on PEDOT:PSS (g) 60 nm thick WO_3 on glass; (h) AgNW 1 on WO_3; (i) AgNW 2 on WO_3. (j) Profile analysis extracted from Figure 3(b); (k) and (l) Height distributions calculated from Figure 3(b), (e) and (g)-(i).

The synthesis of AgNW is typically based on a polyol process, which requires the presence of a polymeric binder like poly(vinylpyrrolidone) (PVP). PVP as well as other polymeric binders are known to environmentally stabilize the AgNW by efficiently cladding them, and further play an essential role as matrix in the film formation properties.[45] The morphologies of AgNW-based IMLs were studied by atomic force microscopy (AFM), as shown in Figures 3(a)-(i). We observed that the formation of the doctor-bladed AgNW layer is strongly affected by the underlying layer. The formation of AgNW coated on top of WO_3 nanoparticles is comparable to that on glass. In contrast, the formation of AgNW will be strongly affected by the underlying PEDOT:PSS layer. The water/IPA-based AgNW solution most likely partially dissolves the PEDOT:PSS layer in the interface, resulting in a mixture of nanowires and nanoparticles. Figure 3(j) depicts the height value along the line in Figure 3(b), indicating that the thickness of the polymeric binder is around 10 nm and the diameters of silver nanowires are ~30 nm.

This picture changes completely for highly diluted AgNW solution. Increasing the dilution with IPA to 1:10 vol% results in a nanoparticular coating, which origins from completely degraded AgNWs. Figure 3(k) depicts the height distributions calculated from the whole area (10×10 µm^2) of Figures 3(b) and (e). The curves present that the height distributions of nanowires (AgNW 1: full square) and nanoparticles (PEDOT:PSS/AgNW 1: full circle) are between 10-60 nm and 30-80 nm respectively, indicating that the maximal height of AgNW above polymer film is ~50 nm, which is supposed to be easily covered by the subsequent 100 nm ZnO-np. By contrast, the formation of AgNW on top of the WO_3 layer is almost the same as that on glass. The roughness (RMS) of WO_3 layer and WO_3/AgNW 2 were measured to be 6.5 and 8 nm on average, respectively. The increase in roughness after blading AgNW 2 on top of WO_3 layer shows great accordance to the roughness of the AgNW 2 layer on glass substrate (2 nm in average). Additionally, the height distributions of Figure 3(g)-(i) are calculated from the whole scanning area (10×10 µm^2) and depicted in the Figure 3(l). After blading the AgNWs thin layer on top of WO_3 the mean value of the height distributions increased from ~56 nm to ~80 nm being in great accordance with the diameters of AgNWs, as shown in Figure 3(j).

To investigate the functionality of AgNW-based IML in a real tandem structure, P3HT:PCBM-based tandem solar cells employing different AgNW-based IMLs were constructed. The J-V characteristics of corresponding tandem solar cells are summarized in Figure S2 and Table S1. By inserting the AgNW between HTL and ETL of the IML, the Voc and FF values of tandem solar cells are significantly improved. The prominent improvements reveal that the AgNW-based IMLs are on the one hand robust enough to protect the underlying active layer from the diffusion of solvents during solution processing of upper layers. On the other hand, these IMLs are also efficient enough to collect the charge carries selectively from sub-cells. It is worthwhile to notice that in our case the combination of PEDOT:PSS/ZnO-np is not robust enough to serve as an eligible IML in the tandem structure. The polymer-matrix of AgNW is not soluble in the nonpolar solvents. Thus, the stability and reliability of IML can be enhanced by inserting the AgNW thin layer. Similar improvements were also observed in the tandem devices employing the WO_3/AgNW 2/ZnO-np intermediate layer. Additionally, tandem solar cells based on PEDOT:PSS/AgNW 2/ZnO-np IML shows a series resistance (Rs) of 1.93 Ω cm^2, which is only slightly higher than the sum-Rs of two sub-cells (1.75 Ω cm^2), indicating that there is almost no extra losses at the interface of this IML. A cross-sectional TEM image of the P3HT:PCBM-based tandem solar cell incorporating the PEDOT:PSS/AgNW/ZnO-np IML is shown in Figure 4.

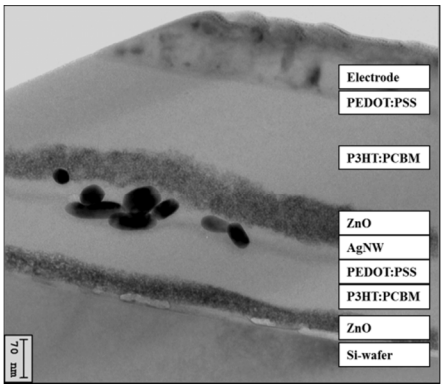

Figure 4 Cross-sectional TEM image of a P3HT:PCBM-based tandem solar cell incorporating the PEDOT:PSS/AgNW/ZnO-np IML.

To demonstrate the advantages of AgNW-based IML on the tandem concept, tandem solar cells based on active layer materials with complementary absorption spectra were constructed. As illustrated in Figure 5(a), the combination of PEDOT:PSS/AgNW 2/ZnO-np was employed as IML for tandem solar cells. Poly[N-9″-hepta-decanyl-2,7-carbazole-alt-5,5-(4′,7′-di-2-thienyl-2′,1′,3′-benzothiadiazole)] (PCDTBT) [48] and a low bandgap diketopyrrolopyrrole-quinquethiophene alternating copolymer (pDPP5T-2) [49,50] were employed as donor materials. The J-V characteristics of tandem solar cell based on PCDTBT:[70]PCBM bottom cell and pDPP5T-2:[60]PCBM top cell, and corresponding reference single cells are summarized in Figure 5(b) and Table 2. The champion tandem solar cell achieved a Voc of 1.44 V along with a Jsc of 8.64 mA/cm2 and FF of 58% resulting in a PCE of 7.25%, while the corresponding reference solar cells obtained a PCE of 5.55% and 5.27% for bottom and top cell respectively. The EQE spectra of tandem and corresponding single cells are depicted in Figure S3. An improvement of >30% in PCE was achieved by incorporating both active layers into a tandem structure, indicating on the one hand the advantage of the tandem concept and on the other hand the promising functionality and reliability of the AgNW based IML. The photovoltaic parameters distribution of 6 tandem solar cells (from one substrate) shown in Figure S4 indicates that Ag nanoparticles were homogeneously deposited and served identically as recombination centres at the interface of HTL/ETL.

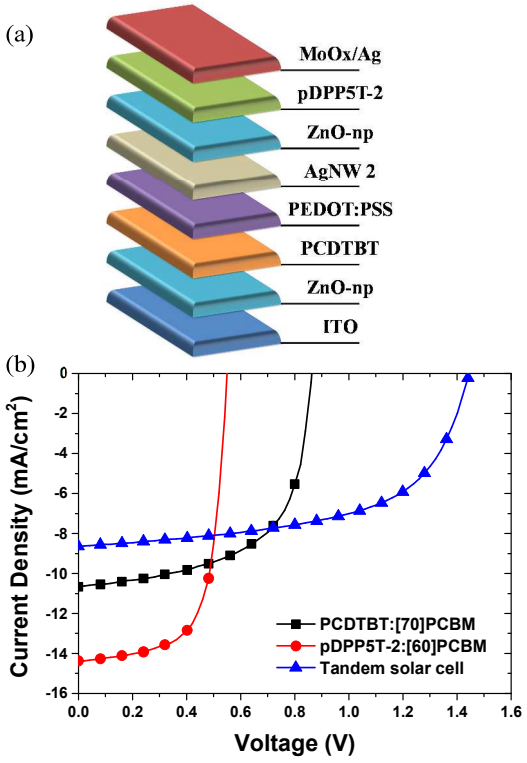

Figure 5 (a) device architecture of tandem solar cells employing AgNW-based IML; (b) J-V characteristics of tandem solar cell based on PCDTBT:[70]PCBM bottom cell and pDPP5T-2:[60]PCBM top cell, and corresponding reference single cells.

Table 2 photovoltaic parameters of tandem solar cell based on PCDTBT:[70]PCBM bottom cell and pDPP5T-2:[60]PCBM top cell, and corresponding reference single cells. A distribution of photovoltaic parameters over 6 tandem solar cells is shown in Figure S3.

	Voc [V]	Jsc [mA/cm^2]	FF [%]	PCE [%]
Ref. Bottom cell	0.87	-10.66	60	5.55
Ref. Top cell	0.55	-14.37	68	5.27
Tandem cell	1.44 (1.46)	-8.64 (-8.55)	58 (58)	7.25 (7.24)

Experimental

Materials: P3HT (Mw=65.5 kg mol−1) and PCDTBT (Mw=127 kg mol^{-1}) were purchased from Merck and St-Jean Photochemicals Inc., respectively. [60]PCBM (99.5%) and [70]PCBM (99%) were purchased from Solenne BV. PEDOT:PSS (Clevios AI4083) was purchased from Heraeus. Silver-nanowire ink and pDPP5T-2 (Mw=47 kg mol−1) were supplied by Cambrios Technology Corporation and BASF, respectively. WO_3 nanoparticles suspension (product no. 4035) was provided by Nanograde Llc. ZnO nanoparticles were synthesized in our lab according to previous publications.[44]

Fabrication of single-junction devices: All the devices were fabricated by doctor-blading under ambient conditions with an architecture shown in Figure 1(a). Pre-structured ITO-coated glass substrates were cleaned in sequence with acetone and isopropyl alcohol (IPA) for 10 minutes. After drying, the substrates were coated with 50 nm thick PEDOT:PSS layer (1:3 vol.% diluted in IPA) or with 60 nm thick WO_3 layer (filtered through a 0.2 µm filter before use) and annealed on a hot plate at 80 °C for 5 min. Afterwards, the AgNW layer (diluted in IPA at 1:5 vol.% for AgNW 1 and 1:10 vol.% for AgNW 2) and ~100 nm thick ZnO-np layer were bladed subsequently and dried at 80 °C for 5 min again. An active layer with a thickness of ~100 nm was bladed from a chlorobenzene solution of P3HT and PCBM with a mixture ratio of 1:1 wt.-%. Then, a diluted solution of PEDOT:PSS (1:5 vol.% in IPA) was bladed on top of active layer. The whole stack was annealed on a hot plate at 140 °C for 5 min after evaporation of a 100 nm thick Ag layer to form the top electrode. For reference, single-junction solar cells based on ZnO-np buffer layer were constructed under the same conditions with an architecture of ITO/ZnO-np/P3HT:PCBM/ PEDOT:PSS/Ag.

Fabrication of tandem solar cells: organic tandem solar cells were fabricated by doctor-blading under ambient conditions with an architecture shown in Figure 5(a). Pre-cleaned ITO coated glass substrates were coated with ~50 nm thick ZnO-np and dried at 80 °C for 5 min. PCDTBT:[70]PCBM (1:4 wt.-% dissolved in dichlorobenzene at a total concentration of 20 mg/mL) with a thickness of ~80 nm was bladed on top of ZnO-np. After that, the IML of PEDOT:PSS/AgNW 2/ZnO-np was bladed on top of the active layer under the same conditions as used for single-junction devices. The second active layer of pDPP5T-2:[60]PCBM (1:2 wt.-% dissolved in a solvent mixture of 95 vol.% chloroform and 5 vol.% dichlorobenzene at a total concentration of 18 mg/mL) with a thickness of ~100 nm was deposited. Afterwards, the whole stack was transferred into a nitrogen-filled glovebox. A 15 nm thick MoOx and a 100 nm thick Ag were thermally evaporated in sequence to form the top electrode.

Characterisations: The active area of OPV devices was defined by the top electrode with a value of 10.4 mm². The J-V characteristics were measured using a source measurement unit from BoTest through a mask with an opening of 10.4 mm^2. Illumination was provided by a solar simulator (Oriel Sol 1A, from Newport) with AM1.5G spectra at 100 mW/cm^2. The optical investigations of thin films were carried out by UV-VIS-NIR spectrometer (Lambda 950, from Perkin Elmer). The thicknesses of films were measured by a profilometer (Tencor Alpha Step D 100). The morphologies of thin films were characterized by AFM (Veeco Model D3100, tapping mode) from the samples prepared on microscopic slides. Sample for cross-sectional TEM was fabricated on a conductive silicon wafer and prepared by focused ion-beam (FIB) sectioning. For FIB sectioning a FEI Strata 235 dual-beam instrument was employed. TEM imaging was performed with an aberration-corrected FEI Titan 80-300. To minimize electron-beam induced damaging of sensitive organic layers the high tension was reduced to 80 kV. [41]

Conclusions

In conclusion, we demonstrated a universal method to fabricate the efficient low-temperature solution-processed IML, in which a solution-processed AgNW-layer was introduced to improve the recombination properties at the interface of HTL/ETL. Due to the limitation of recombination efficiency, the combination of PEDOT:PSS/ZnO-np as well as WO_3/ZnO-np cannot be directly utilized as efficient IMLs for organic tandem solar cells. By inserting an ultra-thin solution-processed AgNW layer, these IMLs showed a similar functionality with the commonly used single buffer layer in single-junction solar cells, indicating that the equivalent ohmic contact was formed between HTL and ETL. With the improvement of recombination properties, single-junction organic solar cells utilizing the combinations of PEDOT:PSS/AgNW/ZnO-np as well as WO_3/AgNW/ZnO-np as IMLs gave PCEs of 2.72 and 3.10% respectively, while the corresponding cells without AgNW showed PCEs of only 1.24 and 0.70% respectively. Furthermore, the AgNW-based IMLs were investigated under the same conditions for P3HT:PCBM-based tandem solar cells, suggesting that the combination of PEDOT:PSS/AgNW 2/ZnO-np can serve as an efficient and robust IML for efficient tandem solar cells. To further verify its functionality and reliability, tandem solar cells based on PCDTBT:[70]PCBM bottom cell and pDPP5T-2:[60]PCBM top cell were constructed. The tandem solar cell achieved a Voc of 1.44V along with a Jsc of 8.64 mA/cm2 and FF of 58% resulting in a PCE of 7.25%.

Acknowledgements

The authors thank Dr. Michael Salinas and Prof. Marcus Halik at the Institute of Polymer Materials (LSP) for the access to AFM measurements, and Christel Dieker and Prof. Erdmann Spiecker at the Center of Nanoanalysis and Electron Microscopy (CENEM) for the help with cross-sectional TEM measurements. Cambrios Technology Corporation and Nanograde are acknowledged for providing the silver-nanowire ink and WO_3 nanoparticles suspension, respectively. The authors thank the support of the Cluster of Excellence "Engineering of Advanced Materials" at FAU, which is funded by the German Research Foundation (DFG) within the framework of its "Excellence Initiative", and the support from "Synthetic Carbon Allotropes" (SFB 953) project and "Solar Technologies Go Hybrid" (SolTech) project.

Notes and references

[a] institute of Materials for Electronics and Energy Technology (i-MEET), Friedrich-Alexander University Erlangen-Nürnberg, Martensstr. 7, 91058 Erlangen, Germany. Email: Ning.Li@fau.de.

[b] BASF Schweiz AG, Schwarzwaldallee 215, CH-4002 Basel, Switzerland.

[c] Bavarian Center for Applied Energy Research (ZAE Bayern), Haberstr. 2a, 91058 Erlangen, Germany.

† Electronic Supplementary Information (ESI) available. See DOI: 10.1039/b000000x/

1. C. J. Brabec, N. S. Sariciftci and J. C. Hummelen, *Advanced Functional Materials*, 2001, **11**, 15-26.
2. C. J. Brabec, *Solar Energy Materials & Solar Cells*, 2004, **83**, 273-292.
3. C. J. Brabec, S. Gowrisanker, J. J. M. Halls, D. Laird, S. Jia and S. P. Williams, *Advanced Materials*, 2010, **22**, 3839-3856.
4. A. J. Heeger, *Advanced Materials*, 2014, **26**, 10-28.
5. F. C. Krebs, N. Espinosa, M. Hösel, R. R. Søndergaard and M. Jørgensen, *Advanced Materials*, 2014, **26**, 29-39.
6. L. Dou, J. You, Z. Hong, Z. Xu, G. Li, R. A. Street and Y. Yang, *Advanced Materials*, 2013, **25**, 6642-6671.
7. M. A. Green, K. Emery, Y. Hishikawa, W. Warta and E. D. Dunlop, *Progress in Photovoltaics: Research and Applications*, 2014, **22**, 1-9.
8. J. You, L. Dou, K. Yoshimura, T. Kato, K. Ohya, T. Moriarty, K. Emery, C.-C. Chen, J. Gao, G. Li and Y. Yang, *Nature Communications*, 2013, **4**, 1446.
9. M. C. Scharber, D. Mühlbacher, M. Koppe, P. Denk, C. Waldauf, A. J. Heeger and C. J. Brabec, *Advanced Materials*, 2006, **18**, 789-794.
10. R. A. J. Janssen and J. Nelson, *Advanced Materials*, 2013, **25**, 1847-1858.
11. N. Li, F. Machui, D. Waller, M. Koppe and C. J. Brabec, *Sol Energ Mat Sol C*, 2011, **95**, 3465-3471.
12. T. Ameri, J. Min, N. Li, F. Machui, D. Baran, M. Forster, K. J. Schottler, D. Dolfen, U. Scherf and C. J. Brabec, *Advanced Energy Materials*, 2012, **2**, 1198-1202.
13. T. Ameri, P. Khoram, J. Min and C. J. Brabec, *Advanced Materials*, 2013, **25**, 4245-4266.
14. L. J. A. Koster, S. E. Shaheen and J. C. Hummelen, *Advanced Energy Materials*, 2012, **2**, 1246-1253.
15. L. Dou, J. You, J. Yang, C.-C. Chen, Y. He, S. Murase, T. Moriarty, K. Emery, G. Li and Y. Yang, *Nature Photonics*, 2012, **6**, 180-185.
16. L. Dou, W.-H. Chang, J. Gao, C.-C. Chen, J. You and Y. Yang, *Advanced Materials*, 2013, **25**, 825-831.
17. J. Jo, J.-R. Pouliot, D. Wynands, S. D. Collins, J. Y. Kim, T. L. Nguyen, H. Y. Woo, Y. Sun, M. Leclerc and A. J. Heeger, *Advanced Materials*, 2013, **25**, 4783-4788.
18. C.-Y. Chang, L. Zuo, H.-L. Yip, Y. Li, C.-Z. Li, C.-S. Hsu, Y.-J. Cheng, H. Chen and A. K. Y. Jen, *Advanced Functional Materials*, 2013, **23**, 5084-5090.
19. W. Li, A. Furlan, K. H. Hendriks, M. M. Wienk and R. A. Janssen, *Journal of the American Chemical Society*, 2013, **15**, 5529-5532.

20. K. Li, Z. Li, K. Feng, X. Xu, L. Wang and Q. Peng, *Journal of the American Chemical Society*, 2013, **135**, 13549-13557.
21. N. Li, D. Baran, G. D. Spyropoulos, H. Zhang, S. Berny, M. Turbiez, T. Ameri, F. C. Krebs and C. J. Brabec, *Advanced Energy Materials*, 2014, **4**, 1400084.
22. T. Ameri, N. Li and C. J. Brabec, *Energ Environ Sci*, 2013, **6**, 2390-2413.
23. G. Dennler, M. C. Scharber, T. Ameri, P. Denk, K. Forberich, C. Waldauf and C. J. Brabec, *Advanced Materials*, 2008, **20**, 579-583.
24. N. Li, T. Stubhan, D. Baran, J. Min, H. Wang, T. Ameri and C. J. Brabec, *Advanced Energy Materials*, 2013, **3**, 301-307.
25. C. J. Brabec, M. Heeney, I. McCulloch and J. Nelson, *Chem Soc Rev*, 2011, **40**, 1185-1199.
26. J. Y. Kim, K. Lee, N. E. Coates, D. Moses, T. Q. Nguyen, M. Dante and A. J. Heeger, *SCIENCE*, 2007, **317**, 222-225.
27. H.-Q. Wang, N. Li, N. S. Guldal and C. J. Brabec, *Organic Electronics*, 2012, **13**, 3014-3021.
28. K. Zilberberg, S. Trost, H. Schmidt and T. Riedl, *Advanced Energy Materials*, 2011, **1**, 377-381.
29. T. Stubhan, T. Ameri, M. Salinas, J. Krantz, F. Machui, M. Halik and C. J. Brabec, *Applied Physics Letters*, 2011, **98**, 253308.
30. K. Zilberberg, H. Gharbi, A. Behrendt, S. Trost and T. Riedl, *ACS Applied Materials & Interfaces*, 2012, **4**, 1164-1168.
31. T. Stubhan, N. Li, N. A. Luechinger, S. C. Halim, G. J. Matt and C. J. Brabec, *Advanced Energy Materials*, 2012, **2**, 1433-1438.
32. N. Li, T. Stubhan, N. A. Luechinger, S. C. Halim, G. J. Matt, T. Ameri and C. J. Brabec, *Organic Electronics*, 2012, **13**, 2479-2484.
33. K. Zilberberg, J. Meyer and T. Riedl, *Journal of Materials Chemistry C*, 2013, **1**, 4796-4815.
34. S. Chen, J. R. Manders, S.-W. Tsang and F. So, *J Mater Chem*, 2012, **22**, 24202-24212.
35. A. Hadipour, B. de Boer, J. Wildeman, F. B. Kooistra, J. C. Hummelen, M. G. R. Turbiez, M. M. Wienk, R. A. J. Janssen and P. W. M. Blom, *Advanced Functional Materials*, 2006, **16**, 1897-1903.
36. S. Sista, M. H. Park, Z. R. Hong, Y. Wu, J. H. Hou, W. L. Kwan, G. Li and Y. Yang, *Advanced Materials*, 2010, **22**, 380-383.
37. C.-H. Chou, W. L. Kwan, Z. Hong, L.-M. Chen and Y. Yang, *Advanced Materials*, 2011, **23**, 1282-1286.
38. K. X. Steirer, P. F. Ndione, N. E. Widjonarko, M. T. Lloyd, J. Meyer, E. L. Ratcliff, A. Kahn, N. R. Armstrong, C. J. Curtis, D. S. Ginley, J. J. Berry and D. C. Olson, *Advanced Energy Materials*, 2011, **1**, 813-820.
39. N. Li, P. Kubis, K. Forberich, T. Ameri, F. C. Krebs and C. J. Brabec, *Sol Energ Mat Sol C*, 2014, **120**, 701-708.
40. J. Krantz, T. Stubhan, M. Richter, S. Spallek, I. Litzov, G. J. Matt, E. Spiecker and C. J. Brabec, *Advanced Functional Materials*, 2013, **23**, 1711-1717.
41. F. Guo, X. Zhu, K. Forberich, J. Krantz, T. Stubhan, M. Salinas, M. Halik, S. Spallek, B. Butz, E. Spiecker, T. Ameri, N. Li, P. Kubis, D. M. Guldi, G. J. Matt and C. J. Brabec, *Advanced Energy Materials*, 2013, **3**, 1062-1067.
42. J.-Y. Lee, S. T. Connor, Y. Cui and P. Peumans, *Nano Letters*, 2008, **8**, 689-692.
43. C.-C. Chen, L. Dou, R. Zhu, C.-H. Chung, T.-B. Song, Y. B. Zheng, S. Hawks, G. Li, P. S. Weiss and Y. Yang, *ACS Nano*, 2012, **6**, 7185-7190.
44. O. Harnack, C. Pacholski, H. Weller, A. Yasuda and J. M. Wessels, *Nano Letters*, 2003, **3**, 1097-1101.
45. S.-H. Zhang, Z.-Y. Jiang, Z.-X. Xie, X. Xu, R.-B. Huang and L.-S. Zheng, *The Journal of Physical Chemistry B*, 2005, **109**, 9416-9421.
46. C. E. Small, S. Chen, J. Subbiah, C. M. Amb, S.-W. Tsang, T.-H. Lai, J. R. Reynolds and F. So, *Nat Photon*, 2012, **6**, 115-120.
47. Z. Liang, Q. Zhang, O. Wiranwetchayan, J. Xi, Z. Yang, K. Park, C. Li and G. Cao, *Advanced Functional Materials*, 2012, **22**, 2194-2201.
48. S. H. Park, A. Roy, S. Beaupre, S. Cho, N. Coates, J. S. Moon, D. Moses, M. Leclerc, K. Lee and A. J. Heeger, *Nature Photonics*, 2009, **3**, 297-302.
49. N. Li, D. Baran, K. Forberich, M. Turbiez, T. Ameri, F. C. Krebs and C. J. Brabec, *Advanced Energy Materials*, 2013, **3**, 1597-1605.
50. N. Li, D. Baran, K. Forberich, F. Machui, T. Ameri, M. Turbiez, M. Carrasco-Orozco, M. Drees, A. Facchetti, F. C. Krebs and C. J. Brabec, *Energ Environ Sci*, 2013, **6**, 3407-3413.

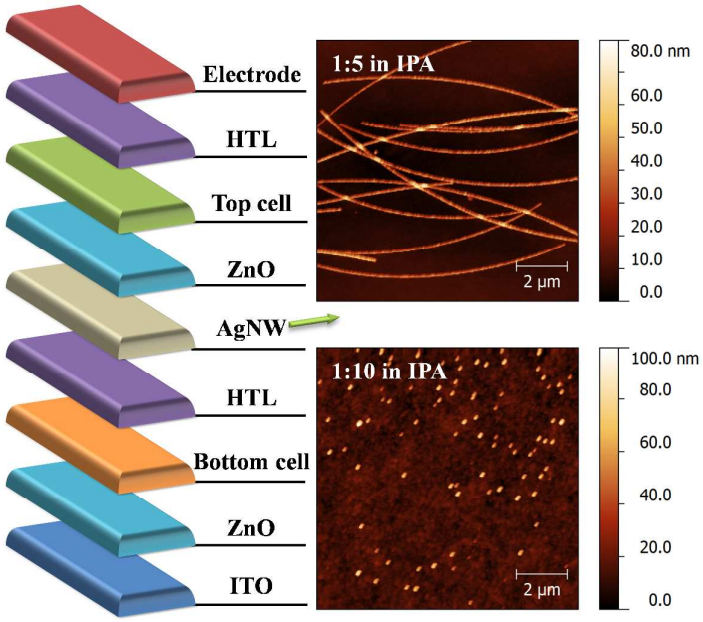

A solution-processed Ag nanostructure based thin layer is introduced to lift the recombination restrictions at the interface of intermediate layer.